UNIVERSITY *of* York

This is a repository copy of *The use of genetic algorithms to maximize the performance of a partially lined screened room*.

White Rose Research Online URL for this paper:
https://eprints.whiterose.ac.uk/674/

White Rose
university consortium
Universities of Leeds, Sheffield & York

eprints@whiterose.ac.uk
https://eprints.whiterose.ac.uk/

The Use of Genetic Algorithms to Maximize the Performance of a Partially Lined Screened Room

Linda Dawson, Janet Clegg, Stuart J. Porter, John F. Dawson, and Martin J. Alexander

Abstract—This paper shows that it is possible to use genetic algorithms to optimize the layout of ferrite tile absorber in a partially lined screened enclosure to produce a "best" performance. The enclosure and absorber are modeled using TLM modeling techniques and the performance is determined by comparison with theoretical normalized site attenuation of free space. The results show that it is possible to cover just 80% of the surface of the enclosure with ferrite absorber and obtain a response which is within ±4 dB of the free space response between 40 and 200 MHz.

Index Terms—Anechoic chamber, ferrite absorber, genetic algorithms, optimization, screened room, transmission line matrix.

I. INTRODUCTION

MOST standards require that radiated emission measurements (in the frequency range 30 to 1000 MHz) are carried out on open field test sites with well-defined performance (usually defined in terms of site attenuation). However, electromagnetic ambients and weather conditions mean that it is difficult to use such a site in many locations. For companies who require their own precompliance test facilities, the next best possibility (an anechoic chamber) is too expensive. An anechoic chamber (AC) which operates down to 30 MHz is either very large, lined with up to 2.5 m depth of carbon-loaded absorber, or is smaller and lined with ferrite tiles. The ferrite tiles are expensive and the room strength required to support the weight of the tiles (of the order of 30 kg/m^2) adds to the cost.

Many companies do not require an enclosure which has the required site attenuation for precompliance and development testing. However, an unlined screened enclosure is sufficiently resonant as to make measurements unrepeatable and results cannot be compared with those obtained in other environments with any degree of confidence. Resonances in an unlined screened room can mean that coupling between a small non-resonant source and a broad-band antenna can change by up to 80 dB over the frequency span of a few megahertz [1]. Also, the field strength measured is highly dependent on the position of the source and the antenna, with a small (e.g., 10 cm) change in the antenna position (for instance) resulting in a change of up to 25 dB in the output.

For these reasons, a partial lining technique was developed at The University of York using analytic and practical methods [1], [2]. The method was developed to allow those without access to anechoic screened enclosures to make usable measurements for precompliance work at frequencies down to 30 MHz. The method relies on reducing the Q of resonances through removing energy from resonant modes by placing lossy material at positions of field maxima. This work showed that it is not necessary to fully line a screened room to obtain a smooth frequency response for coupling between a source and receive antenna. The question then posed is how much material is required (and where should it be placed) to enable the performance of the lined enclosure to be adequate for EMC testing.

It was not possible to use computational techniques to predict the performance of the partial lining technique at the time it was first developed. A method of including the frequency-dependent nature of the reflection from ferrite tiles has been developed for TLM, by one of the authors [3], [4]. This method uses the measured reflectivity of the ferrite to generate a digital filter, which is used to represent the reflectivity of the surface of the material. This allows ferrite lined screened rooms to be efficiently modeled and is described briefly later. The ability to model the ferrite enables the variation in quantity and position of ferrite tiles to be varied to optimize the performance of a partially lined screened room for EMC testing.

The aim of the work described in this paper was to reduce the coverage of lining material from 100% to reduce the cost of an anechoic chamber for full compliance emission testing. It was therefore necessary to optimize the performance of a screened room which was partially lined with ferrite tiles at frequencies below 200 MHz. The choice of ferrite tiles was to allow the use of relatively small rooms at frequencies down to 30 MHz for radiated emission testing. The spaces produced in the tiles were then to be filled with conventional carbon-loaded absorbers which are most effective in the frequency range between 200 MHz and 1 GHz. The modeling and measurements shown in this paper are mostly for the partially lined room with the spaces modeled as perfectly reflecting metal. Some results are included for the situation where the spaces were filled with carbon-loaded absorber. The room dimensions used were 4.76 m × 7.06 m × 4.86 m.

II. FIGURE OF MERIT

Since the final aim of the work was to optimize the tile configuration with an automated computer program, a single figure of merit was required to represent the quality of each tile configuration.
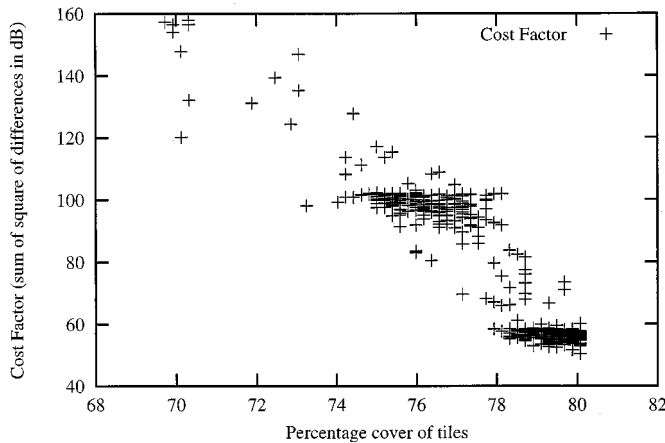
Fig. 1.   Cost factor for a random selection of absorber layouts.

As the aim of the work was to produce a chamber with as near a free space performance as possible (for a given loading of tiles), the figure of merit chosen for this work was generated from the difference between the normalized site attenuation (NSA) in the chamber and the theoretical NSA of free space. The closer the performance to free space, the lower the figure of merit. As a figure of merit usually increases with improved performance rather than decreasing as here, the term "cost factor" will be used instead during the rest of this paper. The cost factor was chosen to reflect the performance over the frequency range 30 to 200 MHz as it is relatively cheap to include carbon-loaded absorbers that will improve the performance of the chamber above this frequency.

Work carried out by others [5] has indicated the use of a figure of merit which uses the sum of three values. These values are the data itself, the first derivative of the data, and the second derivative of the data: the data in this case being the difference between the theoretical free space NSA and the modeled NSA for the chamber. The use of the derivatives is of more use when dealing with rapidly changing data and "peaky" responses. In this case, the data are relatively smooth and it was decided that a simple sum of the differences (in decibels) squared would give an adequate figure, particularly as standards require the site attenuation to be within limits but do not specify any limit on its rate of change. The figure of merit is shown in (1).

Let

$$NSA_f = NSA \text{ of free space}$$
$$NSA_m = NSA \text{ of model}$$
$$Cost = \sum_{frequency} (NSA_m - NSA_f)^2. \qquad (1)$$

The cost factor is shown in Fig. 1 for a random selection of absorber layouts for a single position and polarization with absorber coverage between 70% and 80% of surface area. Although it might be expected that, once a sufficiently high level of coverage had been reached, the cost factor would reach a level where the variation in layout has minimal effect, this is not shown to be the case. Indeed, at 80% coverage, there is still significant variation in the cost factor. As will be shown later, it is possible to obtain a performance within 4 dB of theoretical free space NSA with this level of coverage.

III. GENETIC ALGORITHM

Ferrite tiles are generally 10 cm squares. The size of even a small screened room means that the number of 10-cm-square positions that may be occupied by a tile is of the order of 10 000 (for a 3 m × 3 m × 6 m room). The room under investigation here would need approximately 18 000 tiles. To search manually for the best performance in a problem of this size would be impossible. An automated system is necessary and the use of genetic algorithms is suited for this type of search.

Genetic algorithms are used to search for a solution to a problem which produces a global maximization (or minimization) of the function describing that problem. A set of possible solutions is expressed in a way (such as a binary string) which allows them to be subject to crossover and mutation to generate a new set of possible solutions. Crossover is the swapping of two parts of the string. Before crossover is effected, the first set of possible solutions is evaluated and the results are used to select a subset upon which the crossover is carried out or all the solutions are ranked and the crossover based on this ranking. There are various ways of carrying out the selection and the crossover, as well as introducing "mutations" which increase the probability that the solution is for the global problem (not a local one) by moving the population of solutions out of local minima. The selection used for this work was the "tournament" selection in which two possible solutions are selected at random and the solution with the best cost function is chosen as a parent of the next generation. Both possible solutions are then replaced in the population and two more solutions are selected at random (note that this may select one possible solution more than once and in fact may select good solutions many times) and one is chosen to be another parent in the same way. Tournament selection was used as it has been found to provide a faster convergence than other selection methods for a range of problems [6]. The Cost Factor was monitored during the runs and was found to tend toward the final result without any significant deviations, which implies that the algorithms used were convergent for this particular problem.

Once the parents have been selected, two parents are then "crossed over" to produce two children. In this a random section of the binary string from one parent is removed and replaced with the same part of the string from the second parent (and vice versa) to generate two "children" for the next generation. As the string in this case represented positions on the walls of the enclosure, the portions of the string which were swapped were not contiguous but were chosen to represent rectangular blocks of tiles.

Various proportions of the "parent" population can be replaced by the "children" at each iteration. Again, for speed of convergence, a steady-state algorithm was used. In this case, only 10% of the population was replaced in each generation. The part of the population replaced was chosen by ranking the original population and the new children (which were evaluated) and rejecting the worst 20. The original population consisted of 200 individuals which were chosen to be minor variations around a structure that had been found to give reasonable results in practical work.

To enable the work to be carried out within the time available, the problem space was reduced by dividing the surface area of
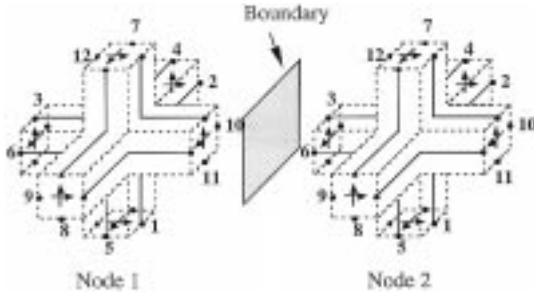
Fig. 2. Symmetrical condensed nodes showing possible placement of reflecting boundary.

the enclosure into 60-cm squares, each one of which was either fully tiled or not tiled. The position of each square was then assigned to a point on the binary string with the 1/0s indicating tiles/no tiles. This significantly reduced the number of possible permutations available and also simplified the problem when the tiles were installed in the enclosure. The use of 60-cm squares also meant that the gaps left between tiles were the correct size for pyramidal absorbers to be included at a later stage without being modified, as the absorbers to be used were 60 cm square.

The possible permutations were also reduced by setting one surface (in this case the ceiling) to be fully tiled. As well as reducing the problem space, this solved two practical problems. The most immediate was the safe attachment and removal of tiles when carrying out measurements on different layouts. The second problem would be more long term in that the completely tiled surface would be the floor to minimize changes in surface level for the easier installation and removal of test equipment. Although the problem space is reduced, it still leaves far too many possibilities to be investigated by hand.

The algorithm might generally be expected to gradually add more tiles as the worst performing patterns were rejected so the algorithm was restricted to reject any patterns with greater than 80% coverage of tiles.

IV. Modeling Technique

This section outlines the transmission line matrix method of numerical electromagnetic analysis, which is very similar to the finite-difference time-domain (FDTD) method. There is no reason why the techniques described below cannot be applied to FDTD. However, the unique boundary description in TLM makes the implementation of the ferrite tiles much simpler.

The transmission line matrix (TLM) method of numerical electromagnetic analysis with the symmetrical condensed node is described in detail in [7]. It is a time-domain code, the results being transformed to obtain the frequency response of the system being modeled. TLM models the propagation of electromagnetic waves in space with a three-dimensional (3-D) mesh of interconnected transmission lines (Fig. 2). Two transmission lines enter each face of a cube of space and carry waves in each of two orthogonal polarizations, giving a total of 12 transmission lines entering the node at the center of the cube. The electric field at each node is proportional to the (vector) sum of the voltages on each transmission line entering the node. The magnetic field is proportional to the sum of the currents on each transmission line entering the node when due consideration is taken for

the direction of magnetic field generated by each line. At each time step, waves entering each node are scattered by the node and become outgoing waves. The scattering is usually described in term of the voltages on each transmission line according to the nodal scattering matrix $\mathbf{S}$

$$
\begin{bmatrix} V_1^r \\ V_2^r \\ \vdots \\ V_{12}^r \end{bmatrix} = \mathbf{S} \cdot \begin{bmatrix} V_1^i \\ V_2^i \\ \vdots \\ V_{12}^i \end{bmatrix}. \tag{2}
$$

The outgoing waves from each node become incoming waves on adjacent nodes and the iteration process can be repeated, e.g., in Fig. 2, if the effects of the boundary are ignored, waves from the adjacent edges of nodes 1 and 2 are exchanged so that

$$
v_3^i = v_{11}^r \qquad v_{11}^i = v_3^r \tag{3a}
$$

and

$$
v_6^i = v_{10}^r \qquad v_{10}^i = v_6^r \tag{3b}
$$

where V^i is incident and V^r is the reflected/scattered field.

The scattering matrix is determined so that energy is conserved and the sum of the fields due to all of the waves obeys Maxwell's equations.

Blocks of material with relative permittivity and permeability greater than one can be represented by loading the transmission lines with open-circuit (capacitive) and short-circuit (inductive) transmission line stubs. These represent the increased permittivity and permeability of the material by adding extra capacitance or inductance to the node. The representation of material conductivity by means of a shunt conductance is described in [8]. The concept of a series resistive element to represent magnetic loss was first proposed in [9] and an improved version developed in [10].

Thin reflective boundaries can be placed between nodes as shown in Fig. 2. The transfer of waves from node to node is therefore affected by the boundary reflection (ρ) and transmission (τ) coefficients so that the connection equations (3) become

$$
v_3^i = \rho v_3^r + \tau v_{11}^r \qquad v_{11}^i = \rho v_{11}^r + \tau v_3^r \tag{4a}
$$

and

$$
v_6^i = \rho v_6^r + \tau v_{10}^r \qquad v_{10}^i = \rho v_{10}^r + \tau v_6^r. \tag{4b}
$$

Boundaries can be used to represent thin walls efficiently in a simulation where the size of each node may be much larger than the wall thickness. For example, a boundary of zero transmission and minus-one reflection coefficient is used to represent the metal walls of an enclosure. The boundary reflection and transmission coefficients are independent of frequency in the standard TLM method.

This technique can be used to model flat plates but is not capable of modeling thin wires so a flat plate model of a 3-D skeletal antenna had to be developed.

A. Representing Ferrite Tiles

Ferrite tile absorbers are made of solid ferrite about 6 mm thick or in a grid construction approximately 20 mm thick. These ferrite tiles cannot be represented accurately over a wide

frequency range with conventional TLM techniques. This is due to the change in their permeability with frequency. They can be represented using the method of [10], but the fine mesh required precludes room modeling due to the very large amount of computer memory required.

These problems have been partially overcome by the development, at York, of a frequency-dependent boundary which accurately models both the phase and amplitude of the reflection coefficient of solid ferrite tiles. This technique can be used with any mesh size to model the action of ferrite absorbing tiles [3].

The formulation is based on the observation that the frequency dependence of ferrite absorbing tiles behaves in a similar manner to the second-order function as

$$F(s) = -\left[\frac{s^2 + 2\zeta\omega_n s + \omega_n^2}{k(s+d)(s+e)}\right] \quad (5)$$

where s is the Laplace variable. The reflection has a minimum magnitude $\rho_{\min}$ when $s = j\omega_n$. The coefficients of the function can be determined from a few points on the reflectivity curve (magnitude only). The equation includes the pole at $s = -e$ to limit the value of reflection coefficient at high frequencies (not considered in [3]). Without this pole, the reflection coefficient could become greater than 1 at higher frequencies.

For large s

$$F(s) \approx -\left[\frac{1}{k}\right] \quad (6)$$

and as s tends to zero

$$F(s) \approx -\left[\frac{\omega_n^2}{kde}\right]. \quad (7)$$

We know that the reflection coefficient for the tile tends to -1 at low frequencies so we can match the functions by taking key points on the reflectivity curve of the ferrite tile. Therefore,

$$\omega_n = 2\pi f_{\min} \quad (8)$$

where $f_{\min}$ is the frequency of the reflection minimum $\rho_{\min}$. The factor k is given by

$$k = \frac{1}{\rho_h} \quad (9)$$

where ρ_h is the magnitude of the reflection coefficient at the highest frequency part of the curve (where the reflection coefficient levels out). The pole e is then determined by

$$e = \frac{2\pi f_u}{k\rho_u} \quad (10)$$

where f_u is the frequency of a point well above the reflection minimum, before the reflection coefficient levels out, and ρ_u is the magnitude of the reflection coefficient at that point. The
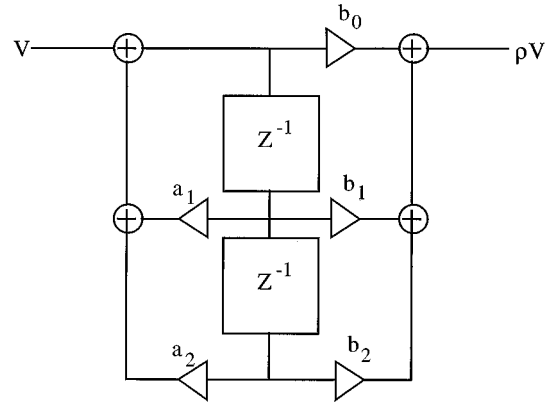

Fig. 3.   Second-order digital filter section used to implement the boundary reflection coefficient.

damping factor ζ can be expressed as a function of earlier factors and the minimum value of the reflectivity $\rho_{\min}$

$$\zeta = \frac{ke\rho_{\min}}{2\omega_n}. \quad (11)$$

The pole position, d, is fixed by the fact that the reflectivity [and hence $F(s)$] must become -1 as s tends to zero so that re-arranging (7) we obtain

$$d = \frac{\omega_n^2}{ke}. \quad (12)$$

The continuous function $F(s)$ can be approximated by the discrete time function

$$H(Z) = \frac{b_0 + Z^{-1}b_1 + Z^{-2}b_2}{1 - a_1 Z^{-1} - a_2 Z^{-2}} \quad (13)$$

where Z^{-1} represents a unit delay. The a and b coefficients can be determined using the impulse invariant transform from $F(s)$ so that

$$a_1 = e^{-dT} + e^{-eT} \quad (14)$$
$$a_2 = -e^{-dT}e^{-eT} \quad (15)$$
$$b_1 = -b_0 \Re(z_{z1} + z_{z2}) \quad (16)$$
$$b_2 = b_0 e^{-(2\zeta\omega_n T)} \quad (17)$$

where $\Re(x)$ indicates the real part of x. The value of b_0 is chosen such that $H(1) = -1$. T is the sample period for the filter which is made equal to the TLM time-step and the zeros, z_{z1} and z_{z2}, of $H(Z)$ are given by

$$z_{z1} = e^{(-\zeta\omega_n T + j\omega_n T\sqrt{1-\zeta^2})} \quad (18a)$$
$$z_{z2} = e^{(-\zeta\omega_n T - j\omega_n T\sqrt{1-\zeta^2})}. \quad (18b)$$

The filter can be implemented as shown in Fig. 3 where V is the incident voltage and ρV is the reflected voltage. Two such filters are required to implement the reflection coefficient at each mesh element boundary, one for each wave polarization.
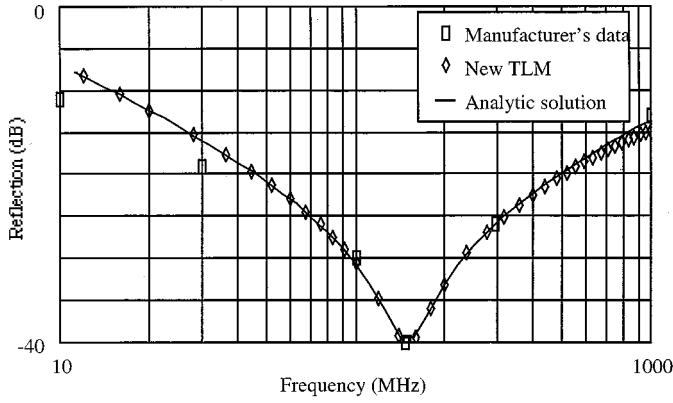
Fig. 4. Modeled reflectivity curve for Philips' tiles compared with analytic and manufacturer's data.

Fig. 5. Difference to theoretical free space NSA for vertical and horizontal polarizations in a room optimized for vertical polarization only.

Results were compared with manufacturer's data and analytical solution of $H(Z)$[1] for results from a 0.1-m TLM mesh for both the conventional flat-tile and the grid-structure ferrite tiles. To compute these results with the material blocks of [9] and [10] would require a mesh size of approximately 1 mm. In many cases, the use of such a fine grid would be impractical due to computer memory limitations.

It was found that the TLM results correspond exactly with the analytical values of $H(Z)$ except for a small deviation in the upper frequency range (Fig. 4). This deviation is due to the roll-off inherent in the TLM mesh impulse response. The TLM results correspond very closely to the manufacturers' data above the reflection minimum but an error of several decibels occurs at low frequencies.

The code used was written at the University of York and is unconditionally stable.

B. Settings for Optimization

To keep the time taken for each model to a minimum, the grid size used was 20 cm. This provides reasonable results up to 200 MHz. The models were run for 512 time steps. This provided sufficient frequency resolution for the damping provided by 80% coverage of tiles which was the requirement. The runs then took 3–4 min each. This meant that the initial run on a population of 200 took approximately 12 h with an additional 1.2 h for the offspring in each generation. The gaps in the tiles were modeled as perfect electrical conductors.

The source used in the models was a single E field excitation of one node. There was no receiving antenna modeled: the output was the predicted field at the required position. The results are all expressed as normalized site attenuation (NSA). This is the site attenuation which has been adjusted for the antenna factors so that measurements made with different antenna sets can in principle be compared. It is thus a measure of the site rather than the antennas. The results are either plotted as NSA or as the difference between the NSA and the theoretical NSA

of free space for the same spacing. The theoretical NSA for free space is given by

$$\text{NSA} = 20 \log_{10} \left(\frac{5 Z_0 D}{2\pi} \right) - 20 \log_{10} f \qquad (19)$$

and includes near field terms which can affect the results at frequencies around 30 MHz with 3-m spacing and where

$$D = \frac{d}{\sqrt{1 - \frac{1}{(\beta d)^2} + \frac{1}{(\beta d)^4}}}$$

with d the separation distance, f is the frequency in megahertz and $\beta = 2\pi/\lambda$.

V. RESULTS

A. Single Antenna Position

Initial runs were carried out for a single source and receive position for horizontal and vertical polarizations individually.

The first run was for a vertical antenna at a height of 2.1 m from the ceiling with the receiving position 3 m from the source at the same height, both being sited on the long axis of the chamber. The source was 2.1 m from one end wall. The optimization process took 170 generations to reduce the cost factor (the sum of the squares of the differences between theoretical NSA and predicted NSA) from 382 to 50.4, and the results of the NSA are shown in Fig. 5. The results appear to be very good with the predicted NSA being within 4 dB of theoretical free space NSA above 34 MHz (maximum excursion 5.5 dB at 30 MHz) and less than 2 dB over most of the frequency band. However, when a prediction on the coupling for a horizontal source and receiving antenna was run for this tile configuration, the results were not as close to the theoretical NSA (Fig. 5). The tile configuration produced here was then used as an initial population for an algorithm to optimize for horizontal polarization. The cost factor was reduced to 52.9 but the tile configuration was different and again performance was not as good for the vertical polarization.

It was, therefore, seen that it was not possible to optimize for both polarizations separately but that the predictions must be

---

[1]It should be noted that $H(Z)$ gives an exact correspondence with the theoretical reflectivity curves obtained from the first-order approximation for the material permeability given in [9].
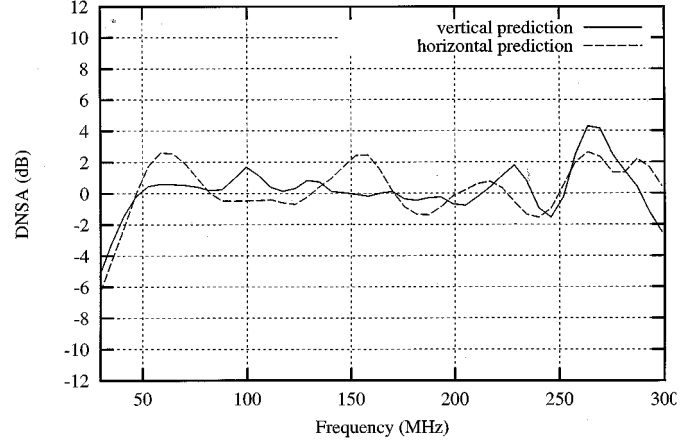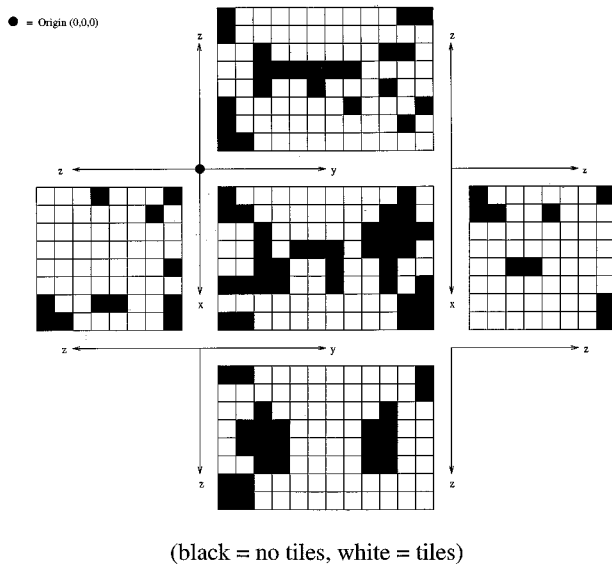
(black = no tiles, white = tiles)

Fig. 6. Optimized layout for four antenna positions and polarizations.
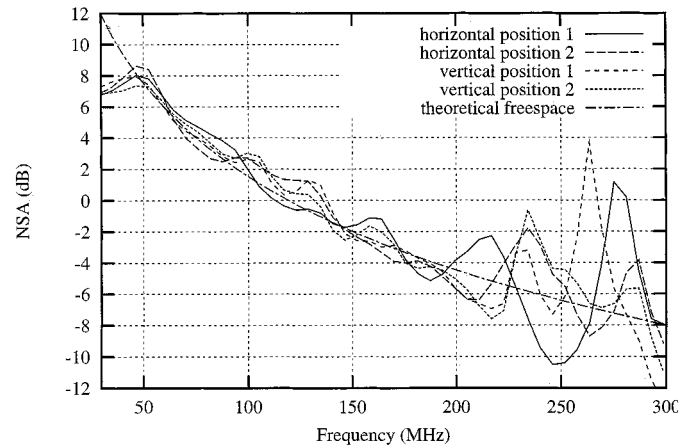

Fig. 7. NSA for each antenna position and polarization with the layout shown in Fig. 6.

Fig. 8. NSA for each antenna position and polarization in a fully lined enclosure.

carried out for both polarizations and the cost factor adjusted to take this into account.

It should be noted that even the fully tiled chamber does not agree with the theoretical free space NSA at 30 MHz although it is within the ±4 dB criterion (Fig. 8).

B. Multiple Antenna Positions

As optimizing for one position and polarization does not optimize for other polarizations and positions, it became necessary to allow for multiple positions of source and receiving antenna in the optimization process. Initially an optimization was carried out with four permutations, i.e., two polarizations and two positions. The next set of runs combined the results for both vertical and horizontal polarizations at antenna heights of 2.1 m and 2.5 m from the ceiling. Source and receive positions were at the same height. To do this, the cost factor was simply changed to be the sum of the cost factors for the individual positions and polarizations. The optimized layout is shown in Fig. 6 with the predicted NSA for the four variations shown in Fig. 7.

The results for this set of four permutations is again very pleasing with the predicted results for all possibilities lying within the 4-dB bound above 34 MHz and within 2 dB between 42 and 200 MHz (Fig. 7). Measurements were carried out for this configuration of tiles and gave good agreement with the predictions. Fig. 8 shows the predicted results for a fully lined chamber with the antennas in the same positions. It is included to show that it is possible to obtain a performance in the partially lined enclosure which is better (i.e., closer to theoretical free space) than the fully lined enclosure over the frequency range for which the chamber was optimized.

In a "real" measurement scenario, the item under test is unlikely to be a point source and could be significantly larger. This means that the source position could effectively be moved to a position where the performance of the lining does not give such a good result. A run was made to optimize the tile layout for a series of positions to overcome this problem. In this case, it was the receive position which was varied as this information could

be obtained from one simulation run and (due to reciprocity) would give the same information as moving the source though the range of positions for a fixed receive point. The transmit position was at a height of 1.9 m from the ceiling so that at no point was the receive position less than 1 m from the ceiling. The receive points were centered on a position 3 m from the source on the center line of the chamber and at the same height. The variation in positions is shown in Fig. 9 and consists of a 15-point grid. The points are spaced 60 cm apart either directly in front or behind the center point or to either side, or at the same positions 80 cm lower and 80 cm higher. The cost factor was modified by summing over each position to give a total cost factor. This optimization run was allowed to proceed for several weeks before being terminated, as the period during which the room would be constructed and measurements made was then imminent. By this time, several hundred generations of evolution had been carried out and it was felt that there would be little lost in damping performance by terminating the program at this point.

The positioning of the source and receive points in the enclosure was chosen to comply with the requirements of the draft concept standard: EN 50147-3 Emission measurements in fully anechoic chambers (1998).
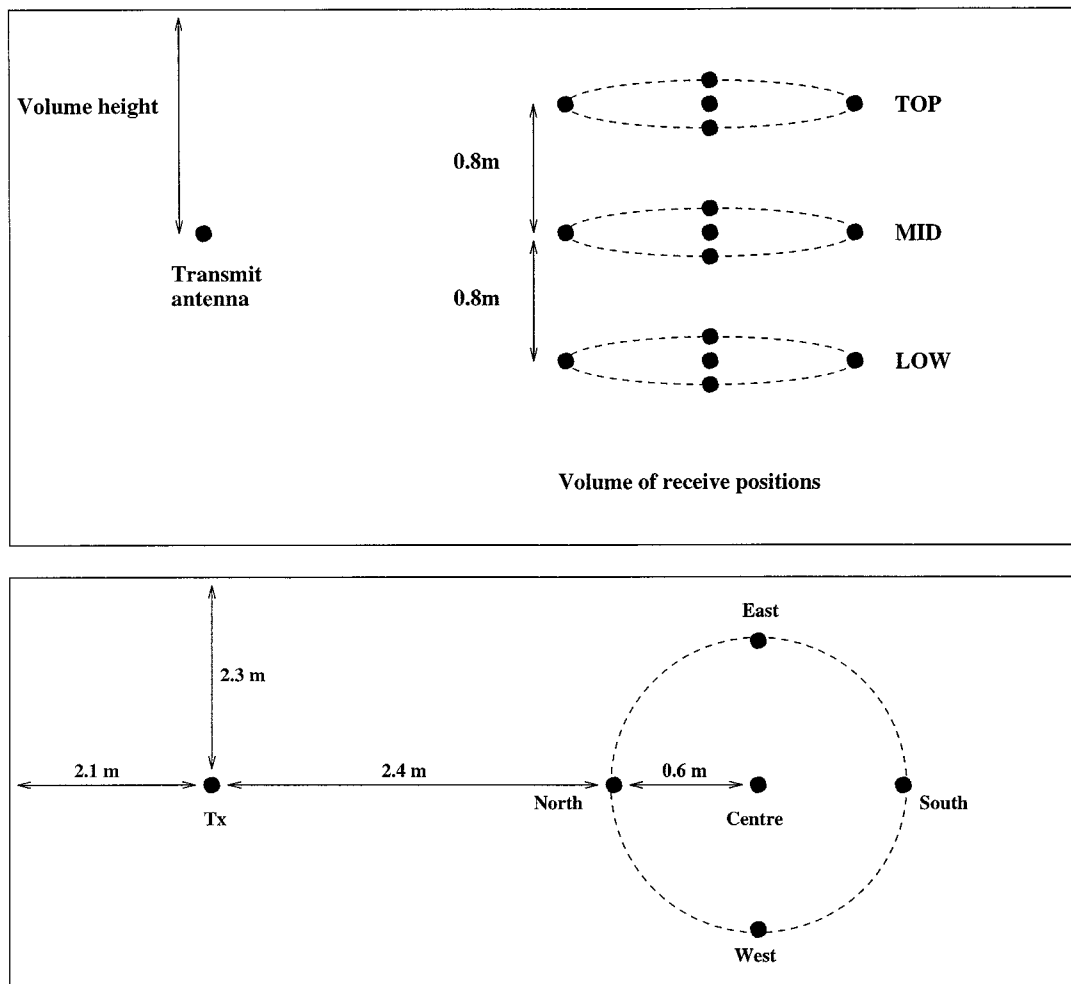
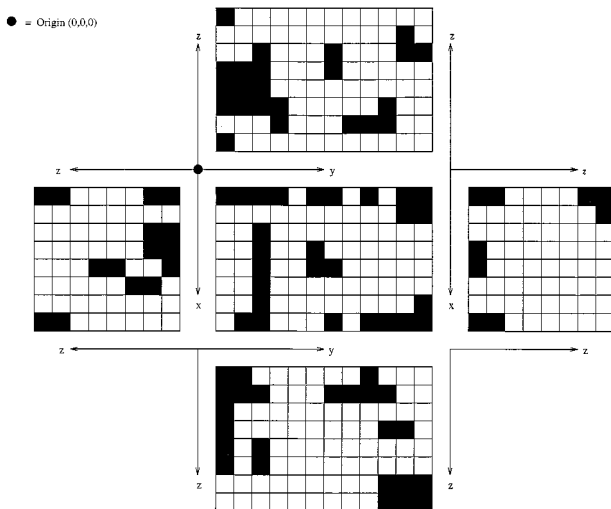Fig. 9. Positions of source and receive for 15-point test volume.

Fig. 10. Final optimized layout for 15-position test volume.

The final layout for tiles (one of many solutions which would give similar results) is shown in Fig. 10. Figs. 11–14 show the predicted and measured results for all 15 positions of the receive point. They are included to show the level of variability in coupling over the possible range of measurement positions.

The predictions indicate that, with vertical polarization, all antenna positions fall within the required performance between 40 MHz and 200 MHz. The horizontal results, however, show a few positions which are up to 1 dB outside the requirements in the same frequency range. It is possible that the fully tiled ceiling (or floor) is the cause and that allowing tiles to be removed from this surface would improve this result. Comparison of the predicted and measured results shows a good agreement over the whole frequency range. Figs. 15 and 16 show the measured and predicted results for one position for both vertical and horizontal positions, again. Again the agreement between predicted and measured results is good with an error of less than 1 dB over most of the frequency range.

The results show both that the performance for the total volume can be made to fall within the required bounds and that the predictions for a single position are very close to the results which may be measured. The final proportion of the surface which was covered with tiles was 81% due to the inclusion of an extra tile on the floor to allow the antenna to be positioned on a flat stable surface.

The results show the responses up to 300 MHz. The results were optimized only up to 200 MHz as it was felt that, beyond this frequency, the addition of relatively low-cost pyramidal absorbers to the gaps between the tiles would improve the perfor-
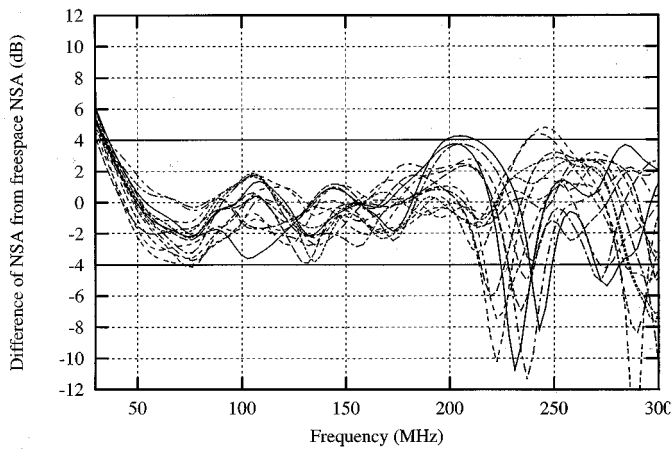
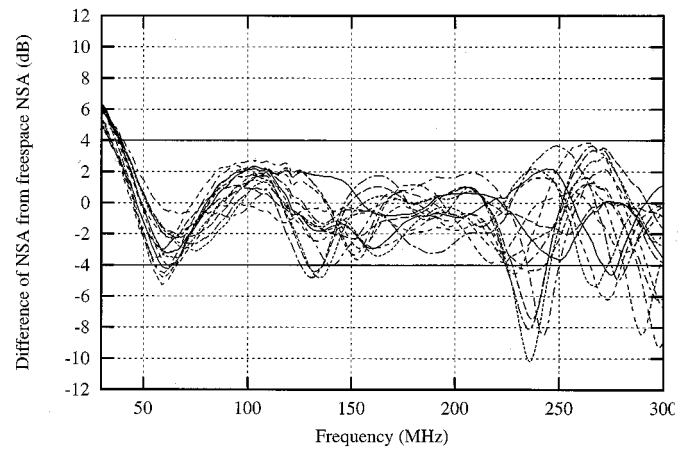Fig. 11. NSA difference from free-space, vertical polarization, modeled for 15 points, optimized chamber.

Fig. 12. NSA difference from free-space, horizontal polarization, modeled for 15 points, optimized chamber.

Fig. 13. NSA difference from free-space, vertical polarization, measured for 15 points, optimized chamber.

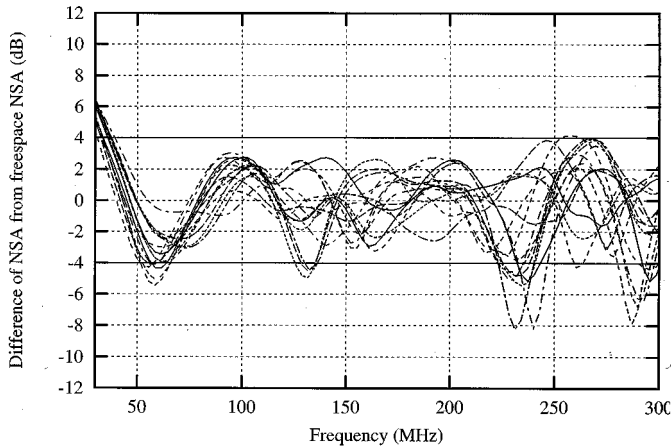Fig. 14. NSA difference from free-space, horizontal polarization, measured for 15 points, optimized chamber.
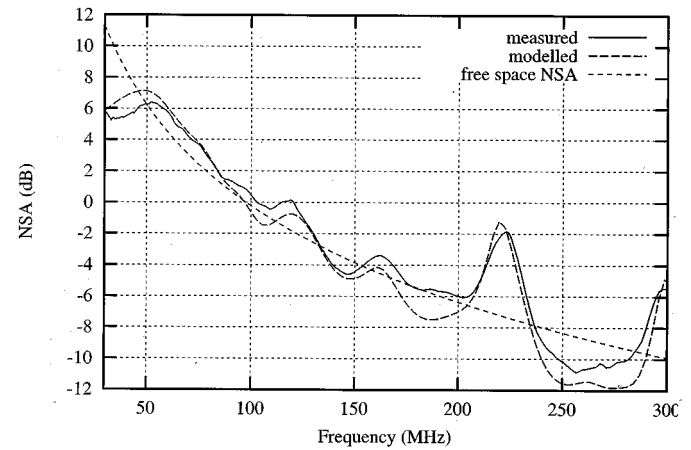

Fig. 15. Measured and predicted NSA for single position (mid north), vertical polarization.
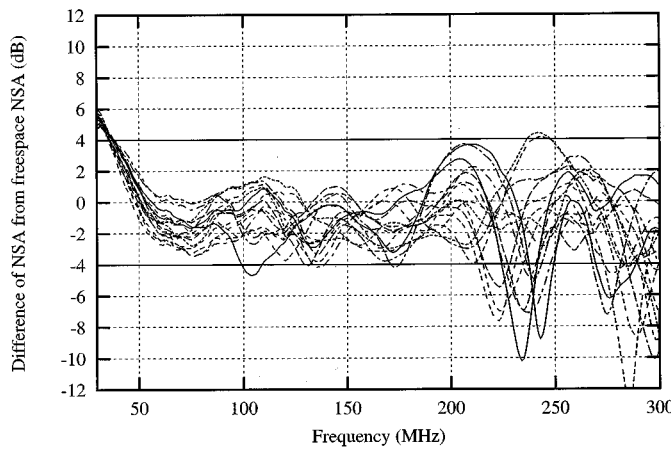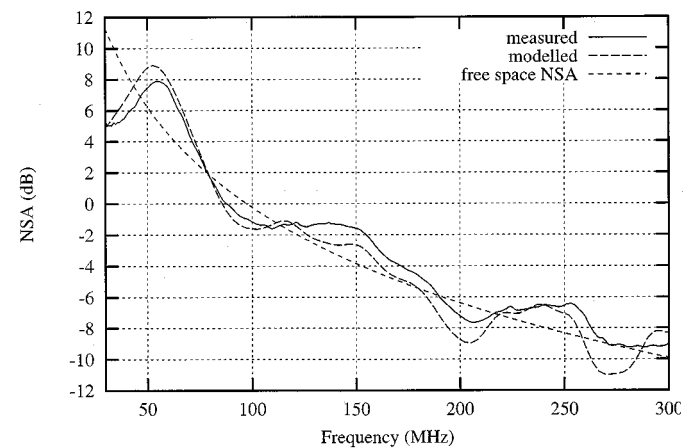

Fig. 16. Measured and predicted NSA for single position (mid north), horizontal polarization, optimized chamber.

mance. Indeed, a model was produced for this type of absorber and included within the optimized room. The results for both the model and practical measurements did bring the performance of the chamber into the required envelope up to 300 MHz (Fig. 17).

Above this frequency, the performance of the models can be expected to degrade due to the grid size being used, but the material performance is good so that there is not expected to be a problem with the NSA between 300 and 1000 MHz. Indeed, measurements bear this out.
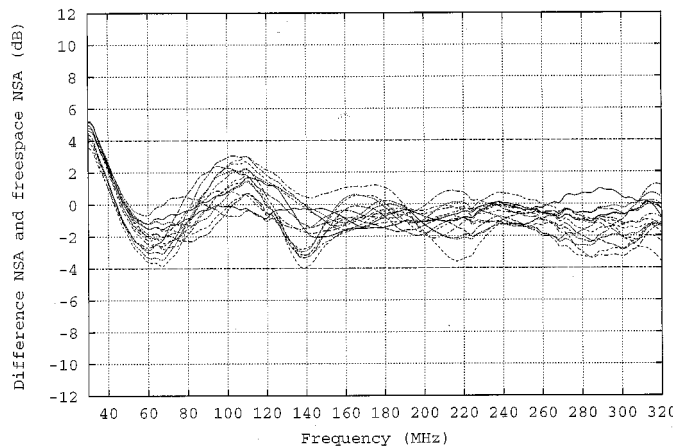
Fig. 17. Measured NSA with a carbon-loaded absorber included for higher frequency performance.

VI. Discussion of Results

The final layout of tiles which was obtained appears to be a quasi-random distribution. Close examination of this distribution appears to show that the gaps in the tiles occur at positions where the modal structure within a resonant enclosure would give low field strengths. However, this enclosure is far from resonant and this is not necessarily a good guide. Indeed, some experimentation was carried out to try to reduce the coverage still further by manually removing tiles which were thought to be at field minima. The results of this experiment generally found that, although the response would not be degraded over a range of frequencies, at a frequency which had not been considered the response would be degraded.

The method of damping resonant enclosures given in [1] and [2] which depends on placing the absorber at modal field maxima works for a much lower coverage of material than is in use for this work. When this quantity of material is included, the modal field structure is no longer the same and cannot be used to determine the absorber position to the same extent.

The programs were run several times with different starting populations. It was found that different patterns were obtained when the runs were terminated. Although they were different, these patterns were similar in that where one had a large area with no tiles others had a similar area. If the program were allowed to run for a much longer time, then the results may converge on one pattern but the improvement in the cost function would be very small and there is unlikely to be one pattern in this range with substantially better performance than the others.

Models were also run with a 1-m cube metal box included within the enclosure. Although this did show a degradation in the results compared to the empty enclosure, this degradation was found to be the same as that experienced in a fully lined room.

VII. Conclusion

It has been shown that it is possible to use genetic algorithms to optimize the layout of absorber in a screened room so that a

"free space" response can be obtained without fully lining the enclosure. The results show good agreement between modeling and measurement for specific positions, which indicates that the modeling method (including that of the ferrite tiles) can be used to investigate this type of environment with a reasonable degree of confidence.

References

[1] L. Dawson and A. C. Marvin, "Methods of damping resonances in a screened room in the frequency range 30 to 200 MHz," in *Proc. EMC Technology Mag. EMC Expo Symp.*, Orlando, FL, June 25–27, 1991, pp. T.4.1–T.4.5.
[2] L. Dawson, J. F. Dawson, A. C. Marvin, and D. Welsh, "Damping resonances within a screened enclosure," *IEEE Trans. Electromagn. Compat.*, vol. 43, pp. 45–55, Feb. 2001.
[3] J. F. Dawson, "Representing ferrite absorbing tiles as frequency dependent boundaries in TLM," *Electron. Lett.*, vol. 29, no. 9, pp. 791–792, 1993.
[4] J. A. Cole, J. F. Dawson, and S. J. Porter, "A digital filter technique for electromagnetic modeling of thin composite layers in TLM," in *Proc. 13th Annu. Rev. Progress in Applied Computational Electromagnetics*, Monterey, CA, Mar. 17–21, 1997, pp. 686–693.
[5] A. J. M. Williams, A. P. Duffy, M. S. Woolfson, and T. M. Benson, "A powerful new technique for the quantitative validation of modeled and experimental data," *Microwave Opt. Technol. Lett.*, vol. 17, no. 5, pp. 686–693, Apr. 1998.
[6] J. M. Johnson and Y. Rahmat-Samii, "Genetic algorithms in engineering electromagnetic," *IEEE Antennas Propagat. Mag.*, vol. 39, pp. 7–21, Aug. 1997.
[7] P. B. Johns, "A symmetrical condensed node for the TLM method," *IEEE Trans. Microwave Theory Tech.*, vol. MTT-35, pp. 370–377, 1987.
[8] P. Naylor and R. A. Desai, "New three dimensional symmetrical condensed lossy node for the solution of electromagnetic wave problems by TLM," *Electron. Lett.*, vol. 26, no. 7, pp. 492–494, 1990.
[9] F. J. German, G. K. Gothard, and L. S. Riggs, "Modeling of materials with electric and magnetic losses with the symmetrical condensed TLM method," *Electron. Lett.*, vol. 26, no. 16, pp. 1307–1308, 1990.
[10] J. F. Dawson, "Improved magnetic loss for TLM," *Electron. Lett.*, vol. 29, no. 5, pp. 467–468, 1993.

Linda Dawson received the B.Sc. and D.Phil. degrees from the University of York, York, U.K., in 1983 and 1990, respectively.

She is a Research Fellow in the Applied Electromagnetics and Electron Optics Research Group at the University of York. After spending eight years carrying out commercial consultancy and testing work, she returned to the research field where her interests are mostly in the area of measurement techniques for EMC.

Janet Clegg received the B.Sc. and D.Phil. degrees from the University of York, York, U.K., in 1988 and 1992, respectively.

She is a Research Fellow with the Applied Electromagnetics Research Group at the Department of Electronics, University of York. Her research interests include numerical electromagnetic modeling, the optimization of test environments such as screened rooms, gtem cells, and stirred mode chambers, optimization of traffic networks using signal design, and the use of genetic algorithms.

Stuart J. Porter received the B.Sc. and D.Phil. degrees from the University of York, York, U.K., in 1985 and 1991, respectively.

He is a Lecturer and member of the Applied Electromagnetics Research Group at the Department of Electronics, University of York. His research interests include computational electromagnetics, particularly as applied to radio-frequency and microwave problems, computational and computer-aided tools for EMC design, antenna design, application of evolutionary computation optimization methods to antenna design and EMC, and computational acoustics.

John F. Dawson received the B.Sc. and D.Phil. degrees from the University of York, York. U.K., in 1982 and 1989, respectively.

He is a Senior Lecturer and member of the Applied Electromagnetics and Electron Optics Research Group in the Department of Electronics, University of York. His research interests include numerical electromagnetic modeling, electromagnetic compatibility prediction for circuits and systems, electromagnetic compatibility test environments, and optimization techniques for EMC design.

Martin J. Alexander received the Honors Degree in physics from Exeter University, U.K., in 1971.

From 1974 to 1988, he worked for the Antenna Division of the GEC-Marconi Research Centre designing transmission line components and antennas in the frequency range 800 MHz to 15 GHz. Since 1988, he has been employed by the National Physical Laboratory, Teddington, U.K., where he designed and developed a facility for the calibration of wire antennas in the VHF and UHF ranges. From 1996 to 1998, he was coordinator of a European project on Fully Anechoic Rooms for EMC testing.

Mr. Alexander is an active member of CISPR/A, contributing to methods of antenna calibration and promoting the calculation of uncertainties in EMC measurements. He is currently working on an opto-electric field transfer standard to transfer the low uncertainties of field strength using the calculable standard dipole into TEM and GTEM cells.